Atmos. Chem. Phys. Discuss., 12, 6909–6955, 2012
www.atmos-chem-phys-discuss.net/12/6909/2012/
doi:10.5194/acpd-12-6909-2012

Atmospheric Chemistry and Physics Discussions

The formaldehyde budget as seen by a global-scale multi-constraint and multi-species inversion system

A. Fortems-Cheiney[1], F. Chevallier[1], I. Pison[1], P. Bousquet[1], M. Saunois[1], S. Szopa[1], C. Cressot[1], T. P. Kurosu[2], K. Chance[3], and A. Fried[4]

[1]Laboratoire des Sciences du Climat et de l'Environnement, CEA-CNRS-UVSQ, UMR8212, Gif-sur-Yvette, France
[2]Jet Propulsion Laboratory, California Institute of Technology, USA
[3]Atomic and Molecular Physics Division, Harvard-Smithsonian Center for Astrophysics, Cambridge, Massachusetts, USA
[4]Earth Observing Laboratory, National Center for Atmospheric Research, Boulder, Colorado, USA

Received: 16 February 2012 – Accepted: 17 February 2012 – Published: 7 March 2012

Correspondence to: A. Fortems-Cheiney (audrey.fortems@lsce.ipsl.fr)

Published by Copernicus Publications on behalf of the European Geosciences Union.

Abstract

For the first time, carbon monoxide (CO) and formaldehyde (HCHO) satellite retrievals have been used together with methane (CH_4) and methyl choloroform (CH_3CCl_3 or MCF) surface measurements in a complex inversion system. The CO and HCHO are, respectively from MOPITT and OMI instruments. The multi-species and multi-satellite dataset inversion is done for the 2005–2008 period. The robustness of our results is evaluated by comparing our posterior-modeled concentrations with several sets of independent measurements of atmospheric mixing ratios. The inversion results lead to significant changes from the prior to the posterior, in terms of magnitude and seasonality of the CO and CH_4 surface fluxes and of the 3-D HCHO production by non-methane volatile organic compounds (NMVOCs). The latter is significantly decreased, indicating an overestimation of the biogenic NMVOCs emissions, such as isoprene, in the GEIA inventory. CO and CH_4 surface emissions are increased by the inversion, from 1037 to 1409 Tg CO and from 489 to 528 TgCH_4 on average for the 2005–2008 period. CH_4 emissions present significant interannual variability and a joint CO–CH_4 fluxes analysis reveals that tropical biomass burning probably played a role in the recent increase of atmospheric methane.

1 Introduction

Formaldehyde (HCHO), found throughout the troposphere, is a short-lived tropospheric gas acting as an outdoor and indoor air pollutant, with a typical lifetime of a few hours in daytime (Sander et al., 2006). HCHO is primarily emitted into the atmosphere by combustion processes, biomass burning (Lee et al., 1998) and vegetation (Lathière et al., 2006). HCHO is also produced in the background troposphere mainly through the chemical oxidation of methane (CH_4) by hydroxyl radicals (OH). In the continental boundary layer, the HCHO source from the oxidation of non-methane volatile organic compounds NMVOCs (i.e., alkanes, alkenes, aromatic hydrocarbons, isoprene)

ACPD
12, 6909–6955, 2012

dominates over the methane oxidation source and can make a large contribution to tropospheric HCHO concentrations. The major sinks of HCHO include oxidation by OH, two photolysis reactions, and dry and wet depositions.

Through its production and loss in the troposphere, HCHO modulates the budget of CH_4 carbon monoxide (CO) and NMVOCs. However, very large uncertainties remain for the relative contributions of these different sources and sinks to the HCHO budget, particularly for the atmospheric production by NMVOCs. This is mainly explained by the diversity of NMVOCs, their short lifetimes, and the large spatio temporal variability of their emissions, leading to large uncertainties of bottom-up estimates (based on emission factors or biogeochemical models). Results of various studies of the global budget of isoprene emissions, which account for about half of the total NMVOCs biogenic source (Guenther et al., 1995), show large discrepancies: the Intergovernmental Panel on Climate Change (IPCC) Working Group on Atmospheric Chemistry and Greenhouse Gases (Ehhalt and Prather, 2001) estimates the isoprene source to 220 $Tg\,yr^{-1}$, whereas it is 3 times higher in Guenther et al. (2006) with 500–750 $Tg\,yr^{-1}$. Closing the formaldehyde budget (including its interactions with CH_4 CO, OH and NMVOCs) is crucial for our understanding of the tropospheric chemistry and for the improvement of emission inventories of HCHO and its precursors.

Complementary to bottom-up estimates, atmospheric inversion offers an approach to optimally infer sources and sinks of an atmospheric species, by tracing back atmospheric signals given by concentration observations to the origin of emissions. It has played an important part during the last decade in the study of CH_4 (Dentener et al., 2003; Bousquet et al., 2006; Bergamaschi et al., 2009) and CO fluxes (Pétron et al., 2004; Pfister et al., 2005; Heald et al., 2004; Tanimoto et al., 2008; Kopacz et al., 2010; Yurganov et al., 2010). Although chemically coupled, the sources and sinks of these trace gases have often been optimized independently from each other. Alternatively, Stavrakou and Müller (2006) have optimized CO emissions by taking into account their relation to NMVOCs and HCHO through OH. Butler et al. (2005) performed a simultaneous mass balance inversion of CH_4 and CO emissions at a low spatial resolution.

ACPD
12, 6909–6955, 2012

Pison et al. (2009) implemented the Simplified Atmospheric Chemistry System (SACS) in a variational inversion system and demonstrated the feasibility of a multi-species inversion, inferring simultaneously CH_4 OH, H_2 and CO sources and sinks. However, these first studies did not use any HCHO observations. Indeed, large disagreements exist between the various measurement techniques employed for measuring HCHO mixing ratios (spectroscopic, chromatographic, and fluorimetric) (Hak et al., 2005). As a result, there is not yet a consistent global measurement network for HCHO, as it exists for greenhouse gases or other air pollutants such as CO, nitrogen oxides (NO_x) and ozone.

These limitations can now be addressed by using HCHO total columns retrieved by satellite, which offer the unique possibility of sensing atmospheric HCHO at a global scale. Past studies have demonstrated the usefulness of HCHO column data (determined in near-UV wavelengths 310–365 nm) from the Global Ozone Monitoring Experiment (GOME) (Abbot et al., 2003; Palmer et al., 2006, 2007; Fu et al., 2007), from the SCanning Imaging Absorption spectroMeter for Atmospheric CartograpHY (SCIAMACHY) (Stavrakou et al., 2009) and from the Ozone Monitoring Instrument (OMI) (Millet et al., 2008) to constrain NMVOCs emissions, the latter having the highest spatial resolution of these 3 instruments. However, none of these studies combine retrievals for various species together.

In this paper, we extend the preliminary work of Pison et al. (2009), Chevallier et al. (2009) and Fortems-Cheiney et al. (2011), and present the first inversion study combining several satellite datasets to constrain the HCHO budget within the same inversion framework, for the years 2005–2008. We simultaneously combine: (i) OMI HCHO columns, (ii) MOPITT CO mixing ratios at 700 hPa, (iii) CH_4 concentrations from the surface networks and (iv) methyl chloroform (MCF) concentrations from the surface networks to constrain OH radicals (Prinn et al., 2001; Krol and Lelieveld, 2003; Bousquet et al., 2005). This paper provides an analysis of the global and regional HCHO budget, with a particular focus on HCHO atmospheric production by NMVOCs. In Sect. 2, the OMI and MOPITT satellite retrievals, and the surface measurements

ACPD
12, 6909–6955, 2012

are briefly presented. The LMDz-SACS chemical-transport model (Sect. 3) is forced by a complex flux scenario and then we apply an atmospheric inversion technique to optimize HCHO sources and sinks against the ensemble of remote and surface data. The main characteristics of our system are summarized in Sect. 4. Section 5 gives the results of the inversion and explores their main features in terms of HCHO budget and implications for the other species (OH, CO and CH_4). The inverted HCHO and CO sources are evaluated by comparison of the optimized and prior concentrations with independent (i.e., not used in the inversion) measurements from aircraft campaigns (INTEX-B, AMMA) and at the surface (NOAA/ESRL, AGAGE, CSIRO, EMPA, SAWS, NIWA and JMA/MRI).

2 Atmospheric constraints

2.1 OMI HCHO retrieved columns

The Ozone Monitoring Instrument (OMI) was launched aboard EOS Aura in July 2004. It has been flying on a 705 km sun-synchronous orbit that crosses the equator at 13:38 LT. OMI is a near-UV/Visible nadir solar backscatter spectrometer covering the spectral range 270–500 nm with a resolution of 0.45 nm between 310 and 365 nm. Its large swath of about 2600 km provides daily global coverage, with a spatial resolution of 13 km × 24 km at nadir, increasing substantially across-track to give an average cross-track spatial resolution of ∼ 43 km. Measured trace gases include O_3, NO_2, SO_2, HCHO, BrO, and OClO (Levelt et al., 2006).

The level 2 data of OMI HCHO Version 3 total columns that we used have been collected from http://mirador.gsfc.nasa.gov/. The data selection follows the criteria of the data quality statement (NASA, 2008): only column values flagged as "good" in the product were included. Also, data with cloud fraction higher than 0.2 were excluded, as recommended by Millet et al. (2006), who showed that the bias on HCHO retrievals decreases with decreasing cloud fraction, from 14 % at a cloud fraction of

ACPD
12, 6909–6955, 2012

0.4 to 6 % at a cloud fraction of 0.2. Similarly, only retrievals between 65° S and 65° N were used in this study. Statistical outliers (column $> 1.0 \times 10^{+19}$ molec cm^{-2}) were also removed. OMI retrievals are affected by an artificial drift, connected to an increase in detector dark current observed over OMI lifetime (Kim et al., 2011), from $2.72 \times 10^{+15}$ molec cm^{-2} in December 2004 to $5.67 \times 10^{+15}$ molec cm^{-2} in December 2008. We have applied an empirical correction developed by the data providers (T. P. Kurosu, personal communication, 2010). It should be noted that the total uncertainties of individual HCHO column retrievals typically range within 50–105 %, with the lower end of this range over HCHO hotspots (Kurosu, 2008).

Due to the scarcity of in situ HCHO measurements, opportunities for validation have been so far limited. The OMI HCHO columns have been evaluated against GOME retrievals by Millet et al. (2008) for the North American region. This study indicates a reasonable agreement between the two datasets: the OMI spatial distribution is similar to that observed by GOME in previous years (differences of 2–14 %), and OMI seems to exhibit less retrieval noise (as seen in their Fig. 2). Boeke et al. (2011) compared OMI HCHO columns to aircraft data over the USA, Mexico, and the Pacific, and found an average bias lower than 3 %.

2.2 MOPITT-V4 CO retrieved mixing ratios

The Measurements Of Pollution In The Troposphere (MOPITT) instrument was launched aboard EOS Terra in December 1999 and it has been operated nearly continuously since March 2000. This spectrometer has flown on a sun-synchronous orbit that crosses the equator at 10:30 and 22:30 LT. The spatial resolution of its observations is about 22 km at nadir. Three days of measurements are needed to achieve global coverage with its 640-km swath.

The Level 2 data of MOPITT Version 4 have been collected from https://wist.echo.nasa.gov/. They include CO mixing ratios at 10 standard pressure levels between the surface and 150 hPa for cloud-free spots. As a trade-off between data volume, closeness to the surface and retrieval noise, only the 700 hPa-level CO retrievals together

ACPD
12, 6909–6955, 2012

with their associated averaging kernels (AK) were used here. Data within 25° from the poles have been left out, as the weight of the a priori CO profile in the MOPITT retrievals increases towards the pole. Night time observations may be biased and were not exploited (Crawford et al., 2004).

MOPITT has been evaluated on a regular basis since the start of the mission in 2000, and compared against aircraft measurements (made during the NASA INTEX-A, NASA INTEX-B and NSF MIRAGE field campaigns), as well as the long-term record from NOAA observations and the MOZAIC experiment (Emmons et al., 2004, 2007, 2009). Retrieval errors are estimated to be about 10 % for each retrieval, with regional biases of a few parts per billion. One should note that the MOPITT retrievals suffer from a time-varying bias in Version 4 (Deeter et al., 2010), as in Version 3 (Yurganov et al., 2008; Emmons et al., 2009; Drummond et al., 2009). This positive bias drifts by about 0.5 ppbv yr^{-1} on average at 700 hPa, in Version 4 (Deeter et al., 2009). This positive bias drift is not taken into account in our observation error and may bias the inversion estimate. Nevertheless, the consistency of the MOPITT-based inverted fluxes with the IASI-based ones showed that the impact of the drift in the MOPITT retrievals is negligible (Fortems-Cheiney et al., 2011).

2.3 Methane and methyl chloroform surface observations

CO, HCHO, CH_4 and OH concentrations are chemically related. OH is an essential modulator of this reaction chain, but this short-lived compound ($\sim$ 1 s) is not easy to constrain in a global atmospheric model. Our approach uses methyl chloroform (CH_3CCl_3 or MCF) as a proxy tracer (Krol and Lelieveld, 2003; Prinn et al., 2005; Bousquet et al., 2005). MCF only reacts with OH and its sources are assumed to be quantified with a rather good accuracy. During the target period of this study (2005–2008), Montzka et al. (2011) showed that the MCF proxy method gives comparable results to CTMs for OH variations. Here, OH monthly 3-D fields are optimized in four latitudinal volumes using a prior spatio-temporal distribution of OH derived from the full LMDz-INCA chemistry climate model (Hauglustaine et al., 2004).

ACPD
12, 6909–6955, 2012

CH_4 in situ measurements are also used, to constrain methane emissions. A set of stations that measured MCF and CH_4 daily or nearly continuously for the 2005–2008 period has been selected from the AGAGE and NOAA/ESRL networks available on the World Data Centre for Greenhouse Gases site (WDCGG, http://gaw.kishou.go.jp/wdcgg/).

3 The LMDz-SACS chemistry transport model

LMDz-SACS is a global 3-D Chemistry Transport Model (CTM) coupling an offline version of the atmospheric general circulation model LMDz (Hourdin et al., 2006) with the atmospheric chemistry module SACS (Simplified Atmospheric Chemistry System) (Pison et al., 2009). To minimize the computational cost of the inversions, we use a pre-calculated archive of 3-hourly transport mass fluxes instead of running the full general circulation model LMDz. The archive has been obtained from a previous simulation of LMDz for the same dates, guided by the horizontal winds analysed by ECMWF. The horizontal resolution is $3.75^\circ \times 2.75^\circ$ and the vertical resolution includes 19 sigma-pressure levels (first level thickness of about 150 m, resolution in the boundary layer of 300 to 500 m and ≈ 2 km at tropopause). The simplification made in SACS compared to INCA (Hauglustaine et al., 2004; Folberth et al., 2006), consists in solving the chemical interaction between a limited set of four species, which represents the oxidation chain of methane: CH_4 HCHO, CO, and OH. The HCHO production and loss in the system are described with the following reactions:

$$CH_4 + OH \rightarrow HCHO \qquad k = 2.45 \times 10^{-12} \exp(-1775/T)\ \mathrm{cm^3\,molec^{-1}\,s^{-1}} \quad (1)$$

$$CH_4 + O^1D \rightarrow HCHO + H_2 \qquad k = 3.75 \times 10^{-11}\ \mathrm{cm^3\,molec^{-1}\,s^{-1}} \quad (2)$$

$$HCHO + OH(+O_2) \rightarrow HO_2 + CO + H_2O$$
$$k = 1.50 \times 10^{-13} \exp(1.06 P/P_0)\ \mathrm{cm^3\,molec^{-1}\,s^{-1}} \quad (3)$$

$$HCHO + h\nu(+O_2) \rightarrow H_2 + CO \qquad J \text{ precomputed by INCA} \quad (4)$$

ACPD
12, 6909–6955, 2012

$$HCHO + h\nu(+O_2) \rightarrow 2HO_2 + CO \quad J \text{ precomputed by INCA} \qquad (5)$$

The prior sources and sinks of formaldehyde, entering or calculated by LMDz-SACS, are summarized in the schematic Fig. 1a, which also depicts part of the SACS mechanism. Averaged over the 4-yr period, the prior photochemical destruction of HCHO is 1210 Tg HCHO yr^{-1} and the surface wet and dry deposition account for 32 Tg HCHO yr^{-1}. The global prior HCHO atmospheric production is 1332 Tg HCHO yr^{-1}, with a contribution of 974 Tg HCHO yr^{-1} from methane oxidation and a contribution of 358 Tg HCHO yr^{-1} from NMVOCs oxidation. Indeed, in addition to the photochemical reactions shown above, the source of HCHO from the degradation of NMVOCs is prescribed in SACS. This 3-D production of formaldehyde is obtained from a previous simulation of the full atmospheric chemistry model LMDz-INCA, using NMVOCs emissions and chemistry of Folberth et al. (2006). In this full-chemistry simulation, the anthropogenic NMVOCs emissions were those from the Emission Database for Global Atmospheric Research (EDGAR-v3.2, http://edgar.jrc.ec.europa.eu) database, valid for 1995 (Olivier and Berdowski, 2001), the biogenic NMVOCs and formaldehyde emissions were taken from the Global Emissions Inventory Activity (GEIA) database (Guenther et al., 1995). Biomass burning emissions were from the interannual Global Fire and Emission database GFED-v2 (Van der Werf et al., 2006) (http://www.globalfiredata.org/).

The sources of the other species, CO and CH_4 including industry and fossil fuel combustion are drawn from the EDGAR-v3.2 and from GFED-v2 inventories. The emissions of CH_4 due to wetlands and termites are based on the study of Fung et al. (1991). It should be noted that we did not adapt the 1995 EDGAR-v3.2 inventory to the 2000s. We choose EDGAR-v3.2 rather than the recent EDGAR-v4.1 for consistency with the study of Fortems-Cheiney et al. (2011).

ACPD
12, 6909–6955, 2012

4 The inverse model

Our inverse problem consists in optimizing the 3-D atmospheric production of formaldehyde, the surface emissions of CO and CH_4 and OH concentrations within the same inversion. We apply the inverse method described by Chevallier et al. (2005, 2007). This inversion scheme uses the LMDz-SACS adjoint model developed by Pison et al. (2009). The optimal solution (in a statistical sense) is found by iteratively minimizing the following cost function:

$$J(\boldsymbol{x}) = (\boldsymbol{x} - \boldsymbol{x}_b)^{\mathrm{T}} \mathbf{B}^{-1} (\boldsymbol{x} - \boldsymbol{x}_b) + (H(\boldsymbol{x}) - \boldsymbol{y})^{\mathrm{T}} \mathbf{R}^{-1} (H(\boldsymbol{x}) - \boldsymbol{y}) \quad (6)$$

where $\boldsymbol{x}$ is the state vector that contains the variables to be optimized by the inversion:

- CO, CH_4 and MCF surface emissions at a $3.75^\circ \times 2.5^\circ$ (longitude, latitude) resolution.
- CO, CH_4 and MCF 3-D initial conditions at an 8-day and at a $3.75^\circ \times 2.5^\circ$ resolution.
- factors to scale the 3-D-chemical production of HCHO (due to NMVOCs) at an 8-day and $3.75^\circ \times 2.5^\circ$ resolution.
- factors to scale the OH atmospheric concentrations at an 8-day resolution, for four latitude bands (90–30° S, 30–0° S, 0–30° N, 30–90° N).

The prior information $\boldsymbol{x}_b$ is a combination of the datasets EDGAR-v3.2, GFED-v2 and GEIA, as described in Sect. 3. The error statistics have been detailed in Fortems-Cheiney et al. (2011) and their main features are recalled here. The covariance matrix **B** of the prior errors is defined as diagonal. The error standard deviations assigned to the CO prior emissions in the covariance matrix **B** are arbitrarily set at 100 % of the maximum value of the emission time series during the corresponding year for each grid point. Errors are set at 100 % of the flux for CH_4 and H_2, at only 1 % of the flux for MCF, at 400 % for the factors to scale the 3-D-chemical production of HCHO and

ACPD
12, 6909–6955, 2012

at 10 % for the scaling factors for the OH atmospheric concentrations. For the initial conditions, errors are set at 10 % for HCHO and MCF and at only 3 % for CH_4 and 5 % for CO. Spatial correlations are defined by an e-folding length of 500 km over land and 1000 km over sea, without any correlation between land and ocean grid points. Temporal correlations are neglected.

The observations in $\boldsymbol{y}$ used for the inversion are surface observations of MCF and CH_4 and satellite data from MOPITT for CO, and from OMI for HCHO (see Sect. 2), both averaged into "super-observations" at the $3.7^\circ \times 2.75^\circ$ resolution of LMDz-SACS, representing about 9.5 millions of constraints for the 2005–2008 time period (see the repartition in Fig. 2). Error correlations between super-observations can be neglected at the $3.75^\circ \times 2.5^\circ$ resolution used for the inversion (Heald et al., 2004), so that the covariance matrix $\mathbf{R}$ of the observation errors is defined as diagonal (i.e., only variances are taken into account). The observation error is the quadratic sum of the measurement error reported in the MOPITT and OMI datasets, and of the CTM errors set to 50 % of the retrieval values according to Pison et al. (2009). Note that for MOPITT, as the averaging kernel (AK) profiles do not vary much within the grid cell, we chose to use the AK profile of the first retrieval when several of them are averaged into a super-observation. Also, it should be noted that there are no averaging kernels associated with the OMI product: the calculation of HCHO model columns is performed as a mean, weighted by the relative thickness of model pressure layers.

For technical reasons, the 4-yr period considered here is processed in consecutive 25-month chunks with a 1 month overlap from one interval to the next. The presence of OH among the optimized variables makes the H operator diverge from linearity and makes the cost function J diverge from quadracity. In this context, the cost function and the norm of its gradient are minimized with the quasi-Newton minimization algorithm M1QN3 (Gilbert and Lemaréchal, 1989), and our system is adapted to deal with non-linearities. After 28 iterations, corresponding to 4 weeks of calculation on 8 processors, the norm of the gradient of the cost function is reduced by 96 %. More iterations do not further reduce the norm of the gradient.

ACPD
12, 6909–6955, 2012

As described by Chevallier et al. (2007), it is possible to rigorously compute the uncertainty of the inverted fluxes by a Monte-Carlo approach. Because of its large computational expense, the computation of the uncertainty on the inverted fluxes was performed for year 2006 only. This resulted in a statistical ensemble of 48 realizations of weekly fluxes, in which the prior and the observations follow their respective error statistics. This ensemble allows computing the flux uncertainty reduction up to the month scale. The monthly flux uncertainty reduction is assumed here to be about the yearly flux uncertainty reduction for HCHO and for CO because of the relatively short lifetime of these species, but this assumption does not hold for CH_4 whose lifetime is about 12 yr (IPCC, 2007). In the following, error bars will therefore be given for HCHO and for CO only.

5 Results

Figure 3 shows the 14 continental regions used to analyse our results.

5.1 HCHO total columns

5.1.1 Comparison to OMI

The OMI observations, the prior, and the posterior-modeled monthly mean global HCHO columns averaged over the 14 continental regions are shown in Fig. 4 for year 2006. The HCHO prior simulated columns and OMI observations show a relatively good agreement regarding both HCHO seasonal cycle and magnitude of concentrations. Except over the boreal and European regions, OMI measures lower concentrations all over the year, compared to the prior simulated concentrations. The largest discrepancies are found over the tropical regions, and particularly over South America and Indonesia. Also, there is a 1-month lag between OMI and the prior concentrations over the regions Eurasian Boreal, North American Boreal and USA: the summer maximum occurs in July for OMI instead of August in the prior concentrations.

ACPD
12, 6909–6955, 2012

In Fig. 4, the HCHO concentrations simulated using our posterior HCHO budgets estimates are plotted in green. Our results show that the inversion succeeds in capturing both the seasonal cycle and the magnitude of the concentrations, improving the fit of the simulations to the observations for the regions USA, South Asia, South East Asia, Australia, South American Temperate, South American Tropical and Indonesia. The 1-month lag seen for the USA and boreal regions is also corrected. However, there are still some discrepancies after inversion: for example, the model fails to reproduce the observed seasonal decrease from July to October for North Africa. This is explained by the relatively large OMI data uncertainties over this region (particularly over Sahara), reaching more than 250 % which implies less deviation from prior fluxes as compared to regions with less uncertain data. Moreover, the agreement for boreal regions is not as good as for other regions because OMI data north of 65° N are not used in the inversion.

5.1.2 Evaluation with independent data

We evaluate the multi-constraint system's performance by comparing our posterior-modeled HCHO concentrations with independent observations. Considering that OMI data integrate the atmospheric column of HCHO, comparison with aircraft observations are of particular interest. The airborne HCHO measurements made during INTEX-B (Intercontinental Chemical Transport ExperimentB) (Singh et al., 2009; Fried et al., 2011) and AMMA (African Monsoon Multidisciplinary Analysis) (Reeves et al., 2010; Borbon et al., 2012) are used for this comparison. The INTEX-B data have been collected in March–May 2006 from aircrafts flying across Mexico and the Gulf coast of the USA (4 March–22 March) and across the Pacific Ocean and the western coastal regions of the USA (17 April–15 May). We compute the ratio of the posterior to the prior bias between modeled and observed concentrations. Locations highlighted in green in Fig. 5, for which ratio is lower than 1, show an improvement of the corresponding statistical indicator after optimization. Over Mexico, the mean bias is reduced by about 4 % (from 2.6 to 2.5 ppb), after the inversion. However, as the prior and posterior simu-

ACPD
12, 6909–6955, 2012

lated concentrations are both in a good agreement with the observations over the USA in March (Fig. 4), target period of the INTEX-B campaign, the ratios of the posterior to the prior bias only range from 0.88 to 1.01 over the Pacific Ocean and the western coastal regions of the USA (Fig. 5, top).

The airborne campaigns AMMA were carried out in August 2006, when the monsoon season was fully developed, across Niamey (Niger). With significant modifications in terms of magnitude and in terms of seasonal variations over Northern Africa, the inversion leads to a dramatic improvement relative to the prior over the Niger, Benin, and Ghana (see Fig. 5, bottom) with a reduction of the mean bias (data minus model) by about 40 % (from 3 to 1.8 ppb).

5.2 Optimization of the HCHO sources and sinks

The optimization of the HCHO column implies changes in the HCHO sources and sinks (surface emissions, atmospheric production and atmospheric loss), which are displayed in Fig. 1b. We do not consider changes of the HCHO surface emissions in the following, as they are very small in magnitude compared to the atmospheric production and loss.

5.2.1 Prior and posterior 3-D HCHO production by NMVOCs

As HCHO is produced by NMVOCs oxidation, and as NMVOCs have sufficiently short lifetimes, there exists a relationship at local scale between the emissions of NMVOCs, their oxidation into HCHO and the observed HCHO column. As a result, the 3-D HCHO production by NMVOCs is a good indicator for the emissions of short-lived NMVOCs (Palmer et al., 2003). The prior and posterior HCHO production by NMVOCs are shown in Table 1 and in Fig. 6. The prior and the posterior uncertainties (1σ) on the 3-D HCHO productio by NMVOCs are presented in Table 1 for year 2006.

The posterior global 4-yr average HCHO production by NMVOCs is estimated at 234 Tg HCHO yr^{-1}, about 35 % lower than the prior estimate (358 Tg HCHO yr^{-1},

ACPD
12, 6909–6955, 2012

Fig. 1b and Table 1). All regions contribute to this decrease even if the changes are smaller for Europe, Middle East and for boreal regions. The main changes are seen over regions of elevated NMVOCs emissions (De Smedt et al., 2008): the USA and South Asia in the Northern Hemisphere, and all tropical regions. We discuss our results for these particular regions in the following.

The annual posterior 3-D HCHO production by NMVOCs is decreased by 32 % over the USA, from 26 Tg HCHO to 18 Tg HCHO on the 4-yr average. As seen in Fig. 6 this decrease only affects the summer months, dominated by enhanced isoprene emissions. Indeed, recent studies (Abbot et al., 2003; Palmer et al., 2003, 2006; Müller et al., 2008) showed that the variability of the HCHO columns over North America reflects the emissions of NMVOCs precursors, and particularly isoprene. Consequently, our results suggest a large overestimation of the isoprene emission over the USA in the GEIA inventory. This is in agreement with the study of Stavrakou et al. (2009). They evaluated the accuracy of the GEIA biogenic emission inventory (502 Tg yr^{-1} for isoprene, 127 Tg yr^{-1} for terpenes, as also used in this study) and the Model of Emissions of Gases and Aerosols MEGAN-ECMWF (Müller et al., 2008) against a new dataset of spaceborne HCHO columns derived from GOME and SCIAMACHY. When they halved the isoprene emissions of the MEGAN-ECMWF inventory over North America (similar to the GEIA's inventory in this particular region), they obtained a significant reduction of their observation to model bias (from 37.2 to 7.6 %). Also, the isoprene emissions inferred by Palmer et al. (2003) from the GOME data are 20 % less than those of GEIA. Shim et al. (2005) recently inverted global isoprene emissions for various ecosystems from September 1996 to August 1997, using the GOME formaldehyde measurements. They also recommended isoprene emission budgets 14 % lower than those of GEIA over the USA, with a reduction for particular ecosystems (grass/shrub, dry evergreen, crop/woods, and the regrowing woods).

In South Asia, the posterior 3-D HCHO production by NMVOCs is half the prior, estimated at 9 Tg HCHO compared to the 18 Tg HCHO of the prior. Figure 6 shows that the prior and the posterior HCHO production by NMVOCs are in a reasonable agreement in

ACPD
12, 6909–6955, 2012

January and in December for this region, when the most abundant source is attributed to anthropogenic activities and particularly to strong domestic heating (Fu et al., 2007). However, for the rest of the year, the posterior HCHO source from NMVOCs is significantly lower than the prior one. Also, the HCHO production by NMVOCs is decreased during the growing season, from April to October. This indicates again an overestimation of the biogenic NMVOCs emission, such as isoprene, in the GEIA inventory.

In Indonesia, the posterior 3-D HCHO production by NMVOCs is largely decreased by the inversion (−60 %), from 26 to 10 Tg HCHO on the 4-yr average. The African continent has a posterior 3-D HCHO production by NMVOCs of 50 Tg HCHO (32 Tg HCHO for Northern Africa and 18 Tg HCHO for Southern Africa), 36 % lower than the prior one.

The inverse modeling results also suggest a much lower HCHO production by NMVOCs, by, respectively 62 % and 39 % for South American Tropical and South American Temperate regions. Their total posterior HCHO production by NMVOCs sources is 15 and 48 Tg HCHO on the 4-yr average. In these 2 regions, it is difficult to disaggregate the biomass burning and biogenic NMVOCs contributions to the observed HCHO signal. However, it can be noticed that Shim et al. (2005) found posterior isoprene emissions 30 % lower than the corresponding GEIA estimate for South America, with a large reduction of the tropical rain forest emissions. The MEGAN- ECMWF biogenic fluxes averaged over the 1997–2011 period are also lower than the GEIA inventory by 40 % (62 vs. 87 Tg HCHO yr^{-1}) (Stavrakou et al., 2009).

By reducing the uncertainty, the inversion has also improved the quality of the 3-D HCHO production by NMVOCs estimates (Table 1). The uncertainty reduction is maximal in the regions South American Temperate (27 %), USA (20 %), South American Tropical, Northern Africa (14 %) and Indonesia (14 %). Significant reductions are also seen for other regions (e.g., 8 % in Western Europe). There is no error reduction in boreal regions (North American Boreal and Eurasian Boreal), due to the lack of OMI data north of 65° N.

ACPD
12, 6909–6955, 2012

The annual 3-D HCHO production range between 214 Tg HCHO yr^{-1} (in 2007) and 256 Tg HCHO yr^{-1} (in 2006), showing significant interannual variability (IAV). Figure 7a shows the regional variation of the 3-D HCHO production by NMVOCs between 2005 and 2008: tropical regions (South American Temperate, South East Asia, Northern Africa and Indonesia) are the main contributors to this IAV. For the regions South East Asia, South American Temperate and Southern Africa to a lesser extent, the lowest is the HCHO production by NMVOCs, the highest are the CO emissions due to biomass burning (e.g., in 2007).

5.2.2 Prior and posterior HCHO production by methane

As the formaldehyde production by methane via the reaction with O^1D is very small (1 % of the global total), we only focus on the HCHO production by methane via the oxidation by OH. The global prior HCHO production by methane is estimated at 974 Tg HCHO yr^{-1}, on the 4-yr average. Due to MCF observations constraining the OH concentrations, and then the loss of methane (via the oxidation into HCHO, Eq. 1), the posterior HCHO production by methane is only 2 % lower than the corresponding prior (946 Tg HCHO yr^{-1}). No change is observed over the regions South American Temp, Middle East, Australia, Indonesia and the USA. The other regions see their HCHO production decreases only by few percents (i.e., −3 % for South East Asia) (not shown).

5.2.3 Prior and posterior HCHO loss

The global posterior HCHO loss is estimated at 1145 Tg HCHO yr^{-1}, 12 % lower than the corresponding prior of 1296 Tg HCHO yr^{-1}, on the 4-yr average (Fig. 1). As a consequence of the reduction of the NMVOCs source, the main changes are seen only for regions that have been impacted by the inversion in terms of HCHO production by NMVOCs (Fig. 6): USA, South Asia and tropical regions.

ACPD
12, 6909–6955, 2012

5.3 Implications for the other species

5.3.1 OH concentrations

Figure 8 copares the global tropospheric mean of the OH concentration between the prior from the fulle chemistry-climate LMDz-INCA model (in red), the posterior derived from Fortems-Cheiney et al. (2011) (using the same inversion framework over the same period, but with only MOPITT-CO satellite data as constraints) and from this study, for the period 2005–2008. The global OH posterior concentration value is 8.59×10^5 mol cm^{-3} on average, 17 % lower than the 10.5×10^5 mol cm^{-3} value of Prinn et al. (2005), and 0.4 % higher than the 8.55×10^5 mol cm^{-3} of Fortems-Cheiney et al. (2011). Figure 9 shows the OH concentration anomalies over the period 2005–2008, relative to the mean. The interannual variability is less than ±4 %, consistent with the low variations reported in Montzka et al. (2011) and compatible with the small IAV inferred by chemistry transport models (Dentener et al., 2003).

The few changes from prior to posterior OH concentrations suggested by the inversion and the small interannual variability of the OH concentrations indicate that the variability of the CO and CH_4 atmospheric concentrations, notably the CH_4 observed atmospheric increase in 2007–2008, are essentially due to the emissions.

5.3.2 CO surface emissions and atmospheric production

The prior and posterior CO surface emissions are presented in Table 2, with their respective uncertainties (1σ) for year 2006. Posterior CO emissions and production from January 2005 to December 2008 reveal higher surface emissions and reduced atmospheric production than the prior estimates (Fig. 1b). The uncertainty reduction is maximal for the South American regions (46 % and 43 %, respectively for South American Tropical and South American Temperate), and for Western Europe (43 %).

The posterior emissions, with a global 4-yr average of 1409 Tg CO yr^{-1}, are 36 % higher than the prior ones, built from the EDGAR-v3.2 and the GFED-v2 inventories

ACPD
12, 6909–6955, 2012

(1037 Tg CO yr^{-1} on average). All regions contribute to this increase of emissions except Northern Africa, South American Tropical, Indonesia and South Asia. Atmospheric production is estimated at 1069 Tg CO yr^{-1}, 12 % lower than the corresponding prior of 1210 Tg CO yr^{-1} (see Sect. 5.2.3).

In terms of budget, these new global emission estimates for the years 2005–2008 are in a good agreement with the results of Fortems-Cheiney et al. (2011), being only 2 % lower (1429 Tg CO yr^{-1} against 1409 Tg CO yr^{-1} on average). Some regions also show a very similar budget between MOPITT-OMI and MOPITT inversions: South Africa (142 and 148 Tg CO yr^{-1} in 2005) and Australia (73 and 78 Tg CO yr^{-1} in 2005). However, there are some differences on emissions (e.g., for the USA with +14 %) due to the decrease of the CO tropospheric production over these regions. We therefore amplify the difference with the North American mass budgets of Kopacz et al. (2010). Our mean value of 150 Tg CO yr^{-1} is much larger than their posterior emissions of 46.5 Tg CO yr^{-1} and also than the study of Hudman et al. (2008). The cause of such a difference is still unclear, but can be due to an underestimation of the CO traffic emissions in the EDGAR-v3.2 inventory (e.g., vehicle cold starts, Parrish, 2006).

On the contrary, we notice that the "MOPITT-OMI"-based emissions are strongly lower than the "MOPITT-only"-based ones in the Middle East region (−50 %, from 75 to 37 Tg CO yr^{-1}) that may be more realistic given the relatively small size of the region and its emission profile This is explained by an increase of the CO atmospheric source. South East Asia region also sees its emissions decrease (by 19 %, from 274 to 221 Tg CO yr^{-1}), reaching a better agreement with the optimized value of 207 Tg CO yr^{-1} from Pétron et al. (2004) and of 169–228 Tg CO yr^{-1} from Carmichael et. (2003). This modification is due to a better fit of the posterior simulated concentrations to the MOPITT observations (not shown).

In terms of interannual variability (IAV), mostly explained by changes in biomass burning emissions and climate (Szopa et al., 2007; Van der Werf et al., 2010), it should be noted that there is no noticeable change between this study and the work of Fortems-Cheiney et al. (2011). The highest regional emissions of the 2005–2008

ACPD
12, 6909–6955, 2012

period are seen for year 2007 (particularly for regions South East Asia and South American Temperate). The lowest estimation of annual CO emissions is calculated for year 2008 with 1337 Tg CO yr^{-1}.

The posterior "MOPITT-OMI" emissions are evaluated for year 2006 by comparing the prior and the posterior modeled CO concentrations with independent (i.e., not used in the inversion) and fixed surface measurements from various networks (NOAA/ESRL, AGAGE, CSIRO, EMPA, SAWS, NIWA and JMA/MRI) available on the WDCGG website. We have restricted our analysis to 39 sites (33 in the Northern Hemisphere presented in Tables 3 and 6 at the high-latitudes of the Southern Hemisphere presented in Table 4) representing remote areas (i.e., Barrow South Pole), or on the contrary, stations close to source regions (i.e., Jungfraujoch, Sonnblick Ryori). We have computed the posterior and the prior bias between the modeled and observed concentrations per station.

The inversion leads to a large improvement relative to the prior simulation for all the stations of Northern Hemisphere with an average reduction of the bias by about 60 %, excepted for the boreal station Ny-Alesund (increase of the bias by 10 %), due to the lack of satellites constraints in the high-latitudes. Moreover, as seen in Table 4 and as already pointed out by Arellano et al. (2004) and by Stavrakou and Müller (2006), the fit is degraded at the high-latitudes Southern Hemisphere sites.

The mean global "MOPITT-OMI" posterior bias is estimated at 11.6 ppb, 10 % lower than the 12.8 ppb mean "MOPITT-only" posterior bias, confirming that the synergistic use of different datasets is required to better quantify CO emissions, even if the improvement is not clearly noticeable for some stations. The largest improvement is seen for the station Sede Boker in Israel (WIS), where the inversion significantly decreases the emissions: the reduction of the bias reached about 80 % compared to the prior and to the "MOPITT-only" simulation.

ACPD
12, 6909–6955, 2012

5.3.3 CH_4 surface emissions

The 4-yr average posterior CH_4 emissions, from January 2005 to December 2008, presented in Table 5, are estimated at 528 $TgCH_4\,yr^{-1}$, higher by 8 % than the corresponding prior (491 $TgCH_4\,yr^{-1}$). Our result is within the range of 500–600 $TgCH_4$ described in IPCC (2007). The main changes between prior and posterior emissions are seen over Northern Africa (+9 %, from 36 to 43 $TgCH_4\,yr^{-1}$ in 2005) and over South Asia (+14 %, from 63 to 71 $TgCH_4\,yr^{-1}$ in 2005). The inversion highlights the importance of the South East Asia region as a CH_4 source with an average of 94 $TgCH_4\,yr^{-1}$, followed by South Asia (73 $TgCH_4\,yr^{-1}$) and South American Temperate (57 $Tg\,CH_4\,yr^{-1}$) regions.

Global CH_4 emissions show significant IAV, with total flux estimates ranging from 512 $TgCH_4$ (in 2006) to 543 $TgCH_4$ (in 2007) (see Table 5). It could be noted that the 2008 global emissions are also high with a total of 538 $TgCH_4\,yr^{-1}$. The largest contributors to the global IAV of CH_4 emissions are the tropical regions (South American Temperate, Northern Africa, South Asia, South East Asia and Indonesia). South America and Asian regions (South + South-East) explain most of the observed atmospheric increase in 2007–2008. Several studies attributed this IAV mostly to natural wetlands (Dlugokencky et al., 2009; Bousquet et al., 2011). Figure 10 shows the variation of the CH_4 posterior emissions and the CO posterior emissions, used as a proxy for biomass burning, over the temperate region South America. This reveals that part of CH_4 flux IAV in this region can be related to biomass burning emissions, at least in 2007. A peak of CH_4 emissions appears to be correlated with a peak of CO emissions in September 2007, and to a lesser extent in September 2005, 2006 and 2008. It should be noted that 2007 was the year of the largest number of fires detected from space over the last ten years (Torres et al., 2010).

The mid-latitude and high-latitude CH_4 emissions (for the regions USA, South American Tropical, Southern Africa, Middle East, Western and Eastern Europe, North American Boreal) seem to vary little from one year to the next (Table 5). However, the

ACPD
12, 6909–6955, 2012

Eurasian Boreal annual budgets show that the 2007 CH_4 emissions are higher than in other years (31 $TgCH_4\,yr^{-1}$, compared with 28 to 30 $TgCH_4\,yr^{-1}$ for years 2005, 2006, 2008). This can be related to higher temperatures complemented by changes in continental precipitations impacting both methane flux densities and wetland extent in 2007 (Dlugokencky et al., 2009; Bousquet et al., 2011).

6 Conclusions

For the first time, an inversion of 3-D HCHO atmospheric production by NMVOCs, carbon monoxide and methane emissions together with OH concentrations, has been performed using a multi-constraint inversion system (using OMI and MOPITT satellite data, surface CH_4 and MCF measurements as constraints). We demonstrated the robustness of our multi-species inversion system to assimilate a large number of data from different types (satellites, surface) over the period 2005–2008.

Significant adjustments in the sources and sinks of formaldehyde are suggested in our study. The large reduction of HCHO concentrations, suggesting a large overestimation of the NMVOCs emissions in the GEIA inventory, leads to a better agreement with the independent INTEX-B and AMMA data. The global posterior 3-D HCHO production by NMVOCs of 234 Tg HCHO is about 35 % lower than the prior estimate of 358 Tg HCHO.

The inversion leads to few changes in the OH concentrations from prior to posterior, and suggests a small interannual variability. This indicates that the variability of the CO and CH_4 atmospheric concentrations, notably the CH_4 observed atmospheric increase in 2007–2008, are primarily due to emissions. The global mean posterior CH_4 emission flux of 528 $TgCH_4\,yr^{-1}$ is 8 % higher than the 490 Tg $CH_4\,yr^{-1}$ of the prior (on a 4-yr average). CH_4 emissions have some significant interannual variability. The joint CO-CH_4 flux analysis suggests that tropical biomass burning probably played a role in the recent variations of atmospheric methane, in South America. The highest annual budget over the period 2005–2008 is calculated in 2007 with 543 $TgCH_4\,yr^{-1}$.

ACPD
12, 6909–6955, 2012

Our inverted global CO surface emission estimate is 1409 Tg CO yr^{-1}, 36 % higher than the corresponding prior but only 2 % lower than the estimate of Fortems-Cheiney et al. (2011) who inverted CO emissions from MOPITT only as constraints. Significant regional changes appeared between the two studies, particularly for Middle East and South East Asia, improving the agreement between the posterior concentrations and independent CO surface data, in comparison to the single use of MOPITT. This highlights how efficient and promising is the synergistic use of MOPITT, OMI and surface measurements for CH_4 and MCF as an adjustment of the prior inventories.

Our conclusions rely on the quality of the HCHO column retrievals. While OMI provides a daily coverage dataset at high spatial resolution, uncertainties remain large for OMI data and the scarcity of in situ measurements remains an issue for evaluation and validation. More efforts should be devoted to the implementation of a common database with uncertainties or a global measurement network for HCHO, as it exists for greenhouse gases or other air pollutants such as CO spanning from urban to remote areas, and from tropical to boreal regions.

Acknowledgements. We acknowledge the KNMI OMI, the NCAR MOPITT, and the NOAA ESRL, Global Monitoring Division (GMD), Halocarbons and other Atmospheric Trace Species (HATS) and Carbon Cycle Greenhouse Gases (CCGG) groups for providing HCHO, CO, MCF and CH_4 measurements. We contacted all data PIs and in particular thank, H. J. R. Wang (AGAGE), J. W. Elkins (NOAA), K. Masarie (NOAA), S. A. Montzka (NOAA), P. C. Novelli (NOAA), E. Dlugokencky (NOAA), P. Krummel (CSIRO), R. Langenfeld (CSIRO), P. Steele (CSIRO), D. Worthy (EC), R. Moss (NIWA), M. Ramonet (LSCE), and G. Brailsford (NIWA). This work was performed using HPC resources of DSM-CCRT and of (CCRT/CINES/IDRIS) under the allocation 2011-t2011012201 made by GENCI (Grand Equipement National de Calcul Intensif). Research at the Smithsonian Astrophysical Observatory was supported by NASA. Finally, we wish to thank F. Marabelle (LSCE) and his team for computer support.

ACPD
12, 6909–6955, 2012

The publication of this article is financed by CNRS-INSU.

References

Abbot, D. S., Palmer, P. I., Martin, R. V., Chance, K. V., Jacob, D. J., and Guenther, A.: Seasonal and interannual variability of North American isoprene emissions as determined by formaldehyde columns measurements from space, Geophys. Res. Lett., 30, 1886, doi:10.1029/2003GL017336, 2003.

Arellano, A., Kasibhatla, P., Giglio, L., Van der Werf, G., and Randerson, J.: Top-down estimates of global CO using MOPITT measurements, Geophys. Res. Lett., 31, L01104, doi:10.1029/2003GL018609, 2004.

Barkley, M. P., Palmer, P. I., Kunh, U., Kesselmeier, J., Chance, K., Kurosu, T. P., Martin, R. V., Helmig, D., and Guenther, A.: Net ecosystem fluxes of isoprene over South America inferred from Global Ozone Monitoring Experiment (GOME) observations of HCHO columns, Geophys. Res., 113, D20301, doi:10.1029/2008JD009863, 2008.

Bergamaschi, P., Frankenberg, C., Meirink, J. F., Krol, M., Villani, M. G., Houweling, S., Dentener, F., Dlugokencky, E. J., Miller, J. B., Gatti, L. V., Engel, A., and Levin, I.: Inverse modeling of global and regional CH_4 emissions using SCIAMACHY satellite retrievals, J. Geophys. Res., 114, D22301, doi:10.1029/2009JD012287, 2009.

Boeke, N. L., Marshall, J. D., Alvarez, S., Chance, K. V., Fried, A., Kurosu, T. P., Rappengluck, B., Richter, D., Walega, J., Weibring, P., and Millet, D. B.: Formaldehyde columns from the ozone monitoring instrument: urban versus background levels and evaluation using aircraft data and a global model, J. Geophys. Res., 116, D05303, doi:10.1029/2010JD014870, 2011.

Bousquet, P., Hauglustaine, D. A., Peylin, P., Carouge, C., and Ciais, P.: Two decades of OH

ACPD
12, 6909–6955, 2012

variability as inferred by an inversion of atmospheric transport and chemistry of methyl chloroform, Atmos. Chem. Phys., 5, 2635–2656, doi:10.5194/acp-5-2635-2005, 2005.
Bousquet, P., Ciais, P., Miller, J. B., Dlugokencky, E. J., Hauglustaine, D. A., Prigent, C., van der Werf, G. R., Peylin, P., Brunke, E.-G., Carouge, C., Langenfeld, R. L., Lathiere, J., Papa, F., Ramonet, M., Schmidt, M., Steele, L. P., Tyler, S. C., and White, J.: Contribution of anthropogenic and natural sources to atmospheric methane variability, Nature, 443, 439–443, doi:10.1038/nature05132, 2006.
Bousquet, P., Ringeval, B., Pison, I., Dlugokencky, E. J., Brunke, E.-G., Carouge, C., Chevallier, F., Fortems-Cheiney, A., Frankenberg, C., Hauglustaine, D. A., Krummel, P. B., Langenfelds, R. L., Ramonet, M., Schmidt, M., Steele, L. P., Szopa, S., Yver, C., Viovy, N., and Ciais, P.: Source attribution of the changes in atmospheric methane for 2006–2008, Atmos. Chem. Phys., 11, 3689–3700, doi:10.5194/acp-11-3689-2011, 2011.
Butler, T. M., Rayner, P. J., Simmonds, I., and Lawrence, M. G.: Simultaneous mass balance inverse modeling of methane and carbon monoxide, J. Geophys. Res., 110(D21), D21310, doi:10.1029/2005JD006071, 2005.
Borbon, A., Ruiz, M., Bechara, J., Aumont, B., Chong, M., Huntrieser, H., Mari, C., Reeves, C.E., Scialom, G., Hamburger, T. , Stark, H., Jambert, A., Mills, G., Perros, P., and Schlager, H.: Transport and chemistry of formaldehyde by mesoscale convective systems in West Africa during AMMA 2006, submitted, J. Geophys. Res., 2012.
Carmichael, G., Tang, Y., Kurata, G., Uno, I., and Streets, D.: Evaluating regional emissions estimates using the TRACE-P observations, J. Geophys. Res., 108(D21), 8810, doi:10.1029/2002JD003116, 2003.
Chevallier, F., Fisher, M., Peylin, P., Serrar, S., Bousquet, P., Breon, F.-M., Chedin, A., and Ciais, P.: Inferring CO_2 sources and sinks from satellite observations: method and application to TOVS data, J. Geophys. Res., 110, doi:10.1029/2005JD006390, 2005.
Chevallier, F., Breon, F.-M., and Rayner, P.: The contribution of the Orbiting Carbon Observatory to the estimation of CO_2 sources and sinks: theoretical study in a variational data assimilation framework, J. Geophys. Res., 112, D24309, doi:10.1029/2006JD007375, 2007.
Chevallier, F., Fortems, A., Bousquet, P., Pison, I., Szopa, S., Devaux, M., and Hauglustaine, D. A.: African CO emissions between years 2000 and 2006 as estimated from MOPITT observations, Biogeosciences, 6, 103–111, doi:10.5194/bg-6-103-2009, 2009.
Crawford, J., Heald, C., Fuelberg, H., Morse, D., Sachse, G., Emmons, L., Gille, J., Edward, D., Deeter, M., Chen, G., Olson, J., Connors, V., Kittaka, C., and Hamlin, A.: Relationship be-

ACPD
12, 6909–6955, 2012

tween measurements of MOPITT and in-situ observations of CO based on a large-scale feature sampled during TRACE-P, J. Geophys. Res., 109, D15S04, doi:10.1029/2003JD004308, 2004.

De Smedt, I., Müller, J.-F., Stavrakou, T., van der A, R., Eskes, H., and Van Roozendael, M.: Twelve years of global observations of formaldehyde in the troposphere using GOME and SCIAMACHY sensors, Atmos. Chem. Phys., 8, 4947–4963, doi:10.5194/acp-8-4947-2008, 2008.

Deeter, M., Edwards, D., Gille, J., Emmons, L., Francis, G., Ho, S.-P., Mao, D., Masters, D., Worden, H., Drummond, J., and Novelli, P.: The MOPITT version 4 CO product: algorithm enhancements, validation, and long-term stability, J. Geophys. Res., 115, D07306, doi:10.1029/2009JD013005, 2010.

Dentener, F., Peters, W., Krol, M., van Weele, M., Bergamaschi, P., and Lelieveld, J.: Interannual variability and trend of CH_4 lifetime as a measure for OH changes in the 1979–1993 time period, J. Geophys. Res.-Atmos., 108, 4442, doi:10.1029/2002JD002916, 2003.

Dlugokencky, E. J., Bruhwiler, L., White, J. W. C., Emmons, L. K., Novelli, P. C., Montzka, S. A., Masarie, K. A., Lang, P. M., Crotwell, A. M., Miller, J. B., and Gatti, L. V.: Observational constraints on recent increases in the atmospheric CH burden, Geophys. Res. Lett, 36, L18803, doi:10.1029/2009GL039780, 2009.

Drummond, J., Zou, J., Nichitiu, F., Kar, J., Deschambaut, R., and Hackett, J.: A review of 9-yr performance and operation of the MOPITT instrument, Adv. Space Res., 45, 6, 760–774, doi:10.1016/j.asr.2009.11.019, 2009.

Ehhalt, D. and Prather, M.: Atmospheric chemistry and greenhouses gases, in: Climate Change 2011: The Scientific Basis, edited by: Houghton, J. T., Ding, Y., Driggsn, D. J., Noguer, M., van der Linden, P. J., Dai, X., Maskell, K., and Johnson, C. A., Cambridge Univ. Press, New York, 2011.

Emmons, L., Deeter, M., Gille, J., Edwards, D., and Attie, J.-L.: Validation of measurements of MOPITT CO retrievals with aircraft in situ profiles, J. Geophys. Res., 109, D03309, doi:10.1029/2003JD004101, 2004.

Emmons, L., Pfister, G., Edwards, D., Gille, J., Sachse, G., Blake, D., Wofsy, S., Gerbig, C., Matross, D., and Nedelec, P.: MOPITT validation exercises during summer 2004 field campaigns over North America, J. Geophys. Res., 112, D12S02, doi:10.1029/2006JD007833, 2007.

Emmons, L. K., Edwards, D. P., Deeter, M. N., Gille, J. C., Campos, T., Nédélec, P., Novelli, P.,

ACPD
12, 6909–6955, 2012

and Sachse, G.: Measurements of Pollution In The Troposphere (MOPITT) validation through 2006, Atmos. Chem. Phys., 9, 1795–1803, doi:10.5194/acp-9-1795-2009, 2009.
Folberth, G. A., Hauglustaine, D. A., Lathière, J., and Brocheton, F.: Interactive chemistry in the Laboratoire de Météorologie Dynamique general circulation model: model description and impact analysis of biogenic hydrocarbons on tropospheric chemistry, Atmos. Chem. Phys., 6, 2273–2319, doi:10.5194/acp-6-2273-2006, 2006.
Fortems-Cheiney, A., Chevallier, F., Pison, I., Bousquet, P., Szopa, S., Deeter, M. N., and Clerbaux, C.: Ten years of CO emissions as seen from Measurements of Pollution in the Troposphere (MOPITT), J. Geophys. Res., 116, D05304, doi:10.1029/2010JD014416, 2011.
Fried, A., Cantrell, C., Olson, J., Crawford, J. H., Weibring, P., Walega, J., Richter, D., Junkermann, W., Volkamer, R., Sinreich, R., Heikes, B. G., O'Sullivan, D., Blake, D. R., Blake, N., Meinardi, S., Apel, E., Weinheimer, A., Knapp, D., Perring, A., Cohen, R. C., Fuelberg, H., Shetter, R. E., Hall, S. R., Ullmann, K., Brune, W. H., Mao, J., Ren, X., Huey, L. G., Singh, H. B., Hair, J. W., Riemer, D., Diskin, G., and Sachse, G.: Detailed comparisons of airborne formaldehyde measurements with box models during the 2006 INTEX-B and MILAGRO campaigns: potential evidence for significant impacts of unmeasured and multigeneration volatile organic carbon compounds, Atmos. Chem. Phys., 11, 11867–11894, doi:10.5194/acp-11-11867-2011, 2011.
Fu, T.-M., Jacob, D. J., Palmer, P. I., Chance, K., Wang, Y. X., Barletta, B., Blake, D. R., Stanton, J. C., and Pilling, M. J.: Space-based formaldehyde measurements as constraints on volatile organic compound emissions in east and south Asia and implications for ozone, J. Geophys. Res., 112, D06312, doi:10.1029/2006JD007853, 2007.
Fung, I., John, J., Lerner, J., Matthews, E., Prather, M., Steele, L. P., and Fraser, P. J.: 3-Dimensional model synthesis of the global methane cycle, J. Geophys. Res., 96(D7), 13033–13065, doi:10.1029/91JD01247, 1991.
Gilbert, J. and Lemaréchal, C.: Some numerical experiments with variable-storage quasi-Newton algorithms, Math. Program., 45, 3, 407–435, 1989.
Guenther, A., Hewitt, C. N., Erickson, D., Fall, R., Geron, C., Graedel, T., Harley, P., Klinger, L., Lerdau, M., McKay, W. A., Pierce, T., Scholes, B., Steinbrecher, R., Tallamraju, R., Taylor, J., and Zimmerman, P.: A global model of natural volatile organic compound emissions, J. Geophys. Res., 100, 8873–8892, 1995.
Guenther, A., Karl, T., Harley, P., Wiedinmyer, C., Palmer, P. I., and Geron, C.: Estimates of global terrestrial isoprene emissions using MEGAN (Model of Emissions of Gases and

ACPD
12, 6909–6955, 2012

Aerosols from Nature), Atmos. Chem. Phys., 6, 3181–3210, doi:10.5194/acp-6-3181-2006, 2006.
Hauglustaine, D. A., Hourdin, F., Jourdain, L., Filiberti, M.-A., Walters, S., Lamarque, J.-F., and Holland, E.: Interactive chemistry in the Laboratoire de Meteorologie Dynamique general circulation model: description and background tropospheric chemistry evaluation, J. Geophys. Res., 109, D04314, doi:10.1029/2003JD003957, 2004.
Hak, C., Pundt, I., Trick, S., Kern, C., Platt, U., Dommen, J., Ordóñez, C., Prévôt, A. S. H., Junkermann, W., Astorga-Lloréns, C., Larsen, B. R., Mellqvist, J., Strandberg, A., Yu, Y., Galle, B., Kleffmann, J., Lörzer, J. C., Braathen, G. O., and Volkamer, R.: Intercomparison of four different in-situ techniques for ambient formaldehyde measurements in urban air, Atmos. Chem. Phys., 5, 2881–2900, doi:10.5194/acp-5-2881-2005, 2005.
Heald, C., Jacob, D., Jones, D., Palmer, P., Logan, J., Streets, D., Sachse, G., Gille, J., Hoffman, R., and Nehrkorn, T.: Comparative inverse analysis of satellite (MOPITT) and aircraft (TRACE-P) observations to estimates Asian sources of carbon monoxide, J. Geophys. Res., 109, D23306, doi:10.1029/2004GL005185 2004.
Hourdin, F., Musat, I., Bony, S., Braconnot, P., and Codron, F.: The LMDZ4 general circulation model : climate performance and sensitivity to parametrized physics with emphasis on tropical convection, Clim. Dynam., 27, 787–813, doi:10.1007/s00382-006-0158-0, 2006.
Hudman, R. C., Murray, L. T., Jacob, D. J., Millet, D. B., Turquety, S., Wu, S., Blake, D. R., Goldstein, A. H., Holloway, J., and Sachse, G. W.: Biogenic versus anthropogenic sources of CO in the United States, Geophys. Res. Lett., 35, L04801, doi:10.1029/2007GL032393, 2008.
IPCC: Climate Change 2007: The Physical Science Basis. Contribution of Working Group I to the Fourth Assessment: Report of the Intergovernmental Panel on Climate Change, edited by: Solomon, S., Qin, D., Manning, M., Chen, Z., Marquis, M., Averyt, K. B., Tignor, M., and Miller, H. L., Cambridge University Press, Cambridge, New York, 996 pp., 2007.
Kim, J. H., Kim, S. M., Baek, K. H., Wang, L., Kurosu, T., De Smedt, I., Chance, K., and Newchurch, M. J.: Evaluation of satellite-derived HCHO using statistical methods, Atmos. Chem. Phys. Discuss., 11, 8003–8025, doi:10.5194/acpd-11-8003-2011, 2011.
Kopacz, M., Jacob, D. J., Fisher, J. A., Logan, J. A., Zhang, L., Megretskaia, I. A., Yantosca, R. M., Singh, K., Henze, D. K., Burrows, J. P., Buchwitz, M., Khlystova, I., McMillan, W. W., Gille, J. C., Edwards, D. P., Eldering, A., Thouret, V., and Nedelec, P.: Global estimates of CO sources with high resolution by adjoint inversion of multiple satellite datasets

ACPD
12, 6909–6955, 2012

(MOPITT, AIRS, SCIAMACHY, TES), Atmos. Chem. Phys., 10, 855–876, doi:10.5194/acp-10-855-2010, 2010.

Krol, M. and Lelieveld, J.: Can the variability in tropospheric OH be deduced from measurements of 1,1,1-trichloroethane (methylchloroform)?, J. Geophys. Res., 108(D3), 4125, doi:10.1029/2002JD002423, 2003.

Kuhn, U., Rottenberger, S., Biesenthal, T., Wolf, A., Schebeske, G., Ciccioli, P., Brancaleoni, E., Frattoni, M., Tavares, T. M., and Kesselmeier, J.: Seasonal differences in isoprene and light-dependent monoterpene emission by Amazonian tree species, Global Change Biol., 10(5), 663–682, doi:10.1111/j.15298817.2003.00771, 2004.

NASA: OMHCHO readme file, available online at: http://disc.sci.gsfc.nasa.gov/Aura/data-holdings/OMI/omhcho_v003.shtml, last access: February 2012, 2008.

Lamarque, J.-F., Bond, T. C., Eyring, V., Granier, C., Heil, A., Klimont, Z., Lee, D., Liousse, C., Mieville, A., Owen, B., Schultz, M. G., Shindell, D., Smith, S. J., Stehfest, E., Van Aardenne, J., Cooper, O. R., Kainuma, M., Mahowald, N., McConnell, J. R., Naik, V., Riahi, K., and van Vuuren, D. P.: Historical (1850–2000) gridded anthropogenic and biomass burning emissions of reactive gases and aerosols: methodology and application, Atmos. Chem. Phys., 10, 7017–7039, doi:10.5194/acp-10-7017-2010, 2010.

Lathière, J., Hauglustaine, D. A., Friend, A. D., De Noblet-Ducoudré, N., Viovy, N., and Folberth, G. A.: Impact of climate variability and land use changes on global biogenic volatile organic compound emissions, Atmos. Chem. Phys., 6, 2129–2146, doi:10.5194/acp-6-2129-2006, 2006.

Lee, M., Heikes, B. G., and Jacob, D. J.: Enhancements of hydroperoxydes and formaldehyde in biomass burning impacted air and their effect on atmospheric oxidant cycles, J. Geophys. Res., 103(D11), 13201–13212, doi:10.1029/98JD00578, 1998.

Levelt, P., Hilsenrath, E., Leppelmeier, G., van den Oord, G., Bhartia, P., Tamminen, J., de Haan, J., and Veefkinf, J.: Science objectives of the ozone monitoring instrument, Geo. Remote Sens., 44, 1199–1208, 2006.

Millet, D. B., Jacob, D. J., Turquety, S., Hudman, R. C., Wu, S., Fried, A., Walega, J., Heikes, B. G., Blake, D. R., Singh, H. B., Anderson, B. E. and Clarke, A. D.: Formaldehyde distributions over North America: Implications for satellite retrievals of formaldehyde columns and isoprene emissions, J. Geophys. Res., 111, D24S02, doi:10.1029/2005JD006853, 2006.

Millet, D. B., Jacob, D. J., Boersma, K. F., Fu, T. M., Kurosu, T. P., Chance, K., Heald, C. L., and Guenther, A.: Spatial distribution of isoprene emissions from North America derived from

formaldehyde column measurements by the OMI satellite sensor, J. Geophys. Res., 113, D02307, doi:10.1029/2007JD008950, 2008.
Montzka, S. A., Krol, M., Dlugokencky, E., Hall, B., Jockel, P., and Lelieveld, J.: Small interannual variability of global atmospheric hydroxyl, Science, 331, 6013, 67–69, doi:10.1126/science.1197640, 2011.
Müller, J.-F., Stavrakou, T., Wallens, S., De Smedt, I., Van Roozendael, M., Potosnak, M. J., Rinne, J., Munger, B., Goldstein, A., and Guenther, A. B.: Global isoprene emissions estimated using MEGAN, ECMWF analyses and a detailed canopy environment model, Atmos. Chem. Phys., 8, 1329–1341, doi:10.5194/acp-8-1329-2008, 2008.
Olivier, J. and Berdowski, J. J. M.: Global emissions sources and sinks, in: The Climate System, Berdowski, J., edited by: Guicherit, R., and Heij, B. J., 33–78, A.A. Balkema Publishers/Swets & Zeitlinger Publishers, Lisse, The Netherlands, ISBN 90 5809 255 0, 2001.
Palmer, P., Jacob, D., Jones, D., Heald, C., Yantosca, R., Logan, J., Sachse, G., and Streets, D.: Inverting for emissions of carbon monoxide from Asia using aircraft observations over the Western Pacific, J. Geophys. Res., 108(D21), 8828, doi:10.1029/2003JD003397, 2003.
Palmer, P., Jacob, D., Jones, D., Heald, C., Yantosca, R., Logan, J., Sachse, G., and Streets, D.: Quantifying the seasonal and interannual variability of North American isoprene emissions using satellite observations of formaldehyde columns, J. Geophys. Res., 111, D12315, doi:10.1029/2005JD006689, 2006.
Palmer, P., Barkley, M. P., Kurosu, T. P., Lewis, A. C., Saxton, J. E., Chance, K., and Gatti, L. V.: Interpreting satellite column observations of formaldehyde over tropcial South America, Phil. Trans. R. Soc. A, 365, 1741–1751, doi:10.1098/rsta.2007.2042, 2007.
Pétron, G., Granier, C., Khattatov, B., Yudin, V., Lamarque, J.-F., Emmons, L., Gille, J., and Edwards, D.: Monthly CO surface sources inventory based on the 2000–2001 MOPITT satellite data, Geophys.Res.Lett, 31, L21107, doi:10.1029/2004GL020560, 2004.
Pfister, G., Hess, P., Emmons, L., Lamarque, J.-F., Wiedinmyer, C., Edwards, D., Pétron, G., Gille, J., and Sachse, G.: Quantifying CO emissions from the 2004 Alaskan wildfires using MOPITT CO data, Geophys. Res. Lett, 32, L11809, doi:10.1029/2005GL022995, 2004.
Pison, I., Bousquet, P., Chevallier, F., Szopa, S., and Hauglustaine, D.: Multi-species inversion of CH_4, CO and H_2 emissions from surface measurements, Atmos. Chem. Phys., 9, 5281–5297, doi:10.5194/acp-9-5281-2009, 2009.
Prinn, R. G., Huang, J., Weiss, R. F., Cunnold, D. M., Fraser, P., Simmonds, P. G., McCulloch, A., Harth, C., Salameh, P., ODoherty, S., Wang, R. H. J., Porter, L., and Miller, B. R.: Evidence

ACPD
12, 6909–6955, 2012

for substantial variations of atmospheric hydroxyl radicals in the past two decades, Science, 292, 5523, 1048–1048, 2001.
Prinn, R. G., Huang, J., Weiss, R. F., Cunnold, D. M., Fraser, P. J., Simmons, P. G., McCulloch, A., Harth, C., Reimann, S., Salameh, P., O'Doherty, S., Wang, R. H. J., Porter, L. W., Miller, B. R., and Krummel, P. B.: Evidence for variability hydroxyl radicals over the past quarter century, Geophys. Res. Lett., 32, L07809, doi:10.1029/2004GL022228, 2005.
Reeves, C. E., Formenti, P., Afif, C., Ancellet, G., Attié, J.-L., Bechara, J., Borbon, A., Cairo, F., Coe, H., Crumeyrolle, S., Fierli, F., Flamant, C., Gomes, L., Hamburger, T., Jambert, C., Law, K. S., Mari, C., Jones, R. L., Matsuki, A., Mead, M. I., Methven, J., Mills, G. P., Minikin, A., Murphy, J. G., Nielsen, J. K., Oram, D. E., Parker, D. J., Richter, A., Schlager, H., Schwarzenboeck, A., and Thouret, V.: Chemical and aerosol characterisation of the troposphere over West Africa during the monsoon period as part of AMMA, Atmos. Chem. Phys., 10, 7575–7601, doi:10.5194/acp-10-7575-2010, 2010.
Sander, S. P., Finalyson-Pitts, B. J., Friedl, R. R., Golden, D. M., Huie, R. E., Keller-Rudeck, H., Kolb, C. E., Kurylo, M. J., Molina, M. J., Moortgat, G. K., Orkin, L. V., Ravishankara, A. R., and Wine, P. H.: Chemical Kinetics and Photochemical data for use in Atmospheric Studies, Evaluation number 15, NASA Panel for data evaluation, JPM Publication 06-2, Jet Propulsion Laboratory, Pasadena, 2006.
Shim, C., Wang, Y., Choi, Y., Palmer, P. I., Abbot, D. S., and Chance, K.: Constraining global isoprene emissions with Global Ozone Monitoring Experiment (GOME) formaldehyde column measurements, J. Geophys. Res., 110, D24301, doi:10.1029/2004JD005629, 2005.
Singh, H. B., Brune, W. H., Crawford, J. H., Flocke, F., and Jacob, D. J.: Chemistry and transport of pollution over the Gulf of Mexico and the Pacific: spring 2006 INTEX-B campaign overview and first results, Atmos. Chem. Phys., 9, 2301–2318, doi:10.5194/acp-9-2301-2009, 2009.
Stavrakou, T. and Müller, J.-F.: Grid-based versus big region approach for inverting CO emissions using MOPITT data, J. Geophys. Res., 111, D15304, doi:10.1029/2005JD006896, 2006.
Stavrakou, T., Müller, J.-F., De Smedt, I., Van Roozendael, M., van der Werf, G. R., Giglio, L., and Guenther, A.: Global emissions of non-methane hydrocarbons deduced from SCIAMACHY formaldehyde columns through 2003–2006, Atmos. Chem. Phys., 9, 3663–3679, doi:10.5194/acp-9-3663-2009, 2009.
Szopa, S., Hauglustaine, D., and Ciais, P.: Relative contributions of biomass burning emissions and atmospheric transport to carbon monoxide interannual variability, Geophys. Res. Lett.,

ACPD
12, 6909–6955, 2012

34, L18810, doi:10.1029/2007GL030231, 2007.
Tanimoto, H., Sawa, Y., Yonemura, S., Yumimoto, K., Matsueda, H., Uno, I., Hayasaka, T., Mukai, H., Tohjima, Y., Tsuboi, K., and Zhang, L.: Diagnosing recent CO emissions and ozone evolution in East Asia using coordinated surface observations, adjoint inverse modeling, and MOPITT satellite data, Atmos. Chem. Phys., 8, 3867–3880, doi:10.5194/acp-8-3867-2008, 2008.
Torres, O., Chen, Z., Jethva, H., Ahn, C., Freitas, S. R., and Bhartia, P. K.: OMI and MODIS observations of the anomalous 2008–2009 Southern Hemisphere biomass burning seasons, Atmos. Chem. Phys., 10, 3505–3513, doi:10.5194/acp-10-3505-2010, 2010.
Trostdorf, C. R., Gatti, L. V., Yamazaki, A., Potosnak, M. J., Guenther, A., Martins, W. C., and Munger, J. W.: Seasonal cycles of isoprene concentrations in the Amazonian rainforest, Atmos. Chem. Phys. Discuss., 4, 1291–1310, doi:10.5194/acpd-4-1291-2004, 2004.
van der Werf, G. R., Randerson, J. T., Giglio, L., Collatz, G. J., Kasibhatla, P. S., and Arellano Jr., A. F.: Interannual variability in global biomass burning emissions from 1997 to 2004, Atmos. Chem. Phys., 6, 3423–3441, doi:10.5194/acp-6-3423-2006, 2006.
van der Werf, G. R., Randerson, J. T., Giglio, L., Collatz, G. J., Mu, M., Kasibhatla, P. S., Morton, D. C., DeFries, R. S., Jin, Y., and van Leeuwen, T. T.: Global fire emissions and the contribution of deforestation, savanna, forest, agricultural, and peat fires (1997–2009), Atmos. Chem. Phys., 10, 11707–11735, doi:10.5194/acp-10-11707-2010, 2010.
van der Werf, G. R., Randerson, J., Giglio, L., Gobron, N., and Dolman, A. J.: Climate controls on the variability of fires in the tropics and subtropics, Global Biogeochem. Cy., 22, GB3028, doi:10.1029/2007GB003122, 2008.
Yurganov, L., McMillan, W., Dzhola, A., Grechko, E., Jones, N., and van der Werf, G.: Global AIRS and MOPITT CO measurements: validation, comparison, and links to biomass burning variations and carbon cycle, J. Geophys. Res., 113, doi:10.1029/2007JD009229, 2008.
Yurganov, L., McMillan, W., Grechko, E., and Dzhola, A.: Analysis of global and regional CO burdens measured from space between 2000 and 2009 and validated by ground-based solar tracking spectrometers, Atmos. Chem. Phys., 10, 3479–3494, doi:10.5194/acp-10-3479-2010, 2010.

ACPD
12, 6909–6955, 2012

Table 1. Total 3-D HCHO production by NMVOCs for years 2005 to 2008 before inversion and **after inversion**, and posterior mean over the 2005–2008 period for 14 continental regions and for the globe in Tg HCHO yr^{-1}. All budgets correspond to a 12-month period. The uncertainty of the inverted fluxes for 2006 are computed by a Monte-Carlo approach. The regional contributions to the global posterior mean are given in % (last column).

	2005		2006		2007		2008		Posterior mean	Contribution (%)
	Prior	Post	Prior	Post	Prior	Post	Prior	Post		
North Am Boreal	4	**3**	4 ± 1	**5 ± 1**	4	**5**	4	**5**	**4**	**2**
USA	26	**16**	26 ± 15	**20 ± 12**	26	**17**	26	**18**	**18**	**8**
South Am Trop	39	**17**	39 ± 19	**19 ± 15**	39	**12**	39	**12**	**15**	**6**
South Am Temp	80	**49**	77 ± 25	**53 ± 10**	77	**44**	81	**47**	**48**	**21**
Northern Africa	50	**28**	49 ± 29	**37 ± 25**	49	**31**	50	**33**	**32**	**14**
Southern Africa	29	**17**	28 ± 18	**21 ± 18**	28	**17**	28	**16**	**18**	**8**
Western Europe	9	**7**	9 ± 5	**9 ± 5**	9	**9**	9	**8**	**8**	**4**
Eastern Europe	6	**4**	6 ± 3	**6 ± 3**	6	**6**	6	**5**	**5**	**2**
Eurasian Boreal	5	**4**	5 ± 1	**6 ± 1**	5	**6**	5	**7**	**6**	**2**
Middle East	3	**3**	3 ± 2	**3 ± 2**	3	**3**	3	**3**	**3**	**1**
South Asia	18	**9**	18 ± 9	**10 ± 8**	18	**8**	18	**9**	**9**	**4**
South East Asia	31	**21**	31 ± 20	**26 ± 19**	31	**22**	32	**22**	**23**	**10**
Indonesia	24	**10**	28 ± 5	**14 ± 4**	28	**9**	23	**8**	**10**	**4**
Australia	15	**10**	16 ± 5	**11 ± 4**	16	**10**	16	**10**	**10**	**4**
Globe	358	**246**	358 ± 58	**257 ± 54**	358	**214**	358	**219**	**234**	**100**

ACPD
12, 6909–6955, 2012

Table 2. Total CO emissions for years 2005 to 2008 before inversion and **after inversion** and posterior mean over the 2005–2008 period for 14 continental regions and for the globe in $Tg\,CO\,yr^{-1}$. The regional contributions to the global posterior mean are given in % (last column). All budgets correspond to a 12-month period. The total estimates include an oceanic CO source amounting to $20\,Tg\,CO\,yr^{-1}$. The uncertainty of the inverted fluxes for 2006 are computed by a Monte-Carlo approach.

	2005		2006		2007		2008		Posterior mean	Contribution (%)
	Prior	Post	Prior	Post	Prior	Post	Prior	Post		
North Am Boreal	11	**62**	9 ± 13	**54 ± 8**	7	**57**	7	**50**	**56**	**4**
USA	116	**149**	117 ± 19	**151 ± 18**	119	**149**	117	**150**	**150**	**11**
South Am Trop	36	**23**	34 ± 12	**24 ± 6**	38	**23**	36	**21**	**23**	**2**
South Am Temp	116	**181**	66 ± 23	**147 ± 13**	121	**230**	60	**165**	**181**	**13**
Northern Africa	154	**98**	141 ± 23	**100 ± 14**	161	**80**	144	**82**	**90**	**6**
Southern Africa	107	**142**	92 ± 21	**134 ± 13**	96	**149**	104	**145**	**142**	**10**
Western Europe	70	**94**	70 ± 13	**91 ± 7**	70	**89**	69	**86**	**90**	**6**
Eastern Europe	40	**68**	41 ± 15	**70 ± 10**	39	**65**	40	**59**	**65**	**5**
Eurasian Boreal	18	**90**	30 ± 22	**99 ± 16**	20	**134**	41	**129**	**113**	**8**
Middle East	24	**38**	24 ± 10	**36 ± 7**	24	**35**	24	**39**	**37**	**3**
South Asia	80	**72**	80 ± 16	**65 ± 11**	80	**49**	80	**51**	**61**	**4**
South East Asia	168	**213**	168 ± 20	**213 ± 15**	201	**257**	164	**202**	**221**	**16**
Indonesia	87	**73**	129 ± 5	**121 ± 4**	44	**29**	45	**30**	**63**	**4**
Australia	18	**78**	29 ± 14	**91 ± 10**	25	**119**	18	**100**	**79**	**6**
Globe	1066	**1401**	1047 ± 68	**1414 ± 66**	1065	**1484**	969	**1337**	**1409**	**100**

ACPD
12, 6909–6955, 2012

Table 3. Statistics of the fit for the 33 stations chosen in the Northern Hemisphere. Bias is defined as the mean difference between observed and modeled CO concentrations (model-minus-observation, average over the year 2006). The "MOPITT-only posterior" bias is given by Fortems-Cheiney et al. (2011). The lowest bias for each station is highlighted in bold.

Code	Location	Biais (ppb)		
		Prior	Posterior	MOPITT-only posterior
ALT	Alert, Canada	−25.8	17.0	**13.1**
ASC	Ascension Island, UK	−7.7	**−0.6**	−07
ASK	Assekrem, Algeria	−18.9	−10.1	**−6.4**
AZR	Terceira Island, Portugal	−29.8	−9.2	**−7.7**
BMW	Tudor Hill, IK	−12.5	**−11.7**	12.5
BRW	Barrow, USA	−28.5	20.3	**17.5**
BSC	Black Sea, Romania	−38.7	4	**3.6**
CBA	Cold Bay, USA	−33.6	11.2	**10.8**
CHR	Christmas Island, Kiribati	−7.8	**−5.5**	−5.7
EIC	Easter Island, Chile	−9.0	2.1	**1.3**
GMI	Mariana Islands, Guam	−23.6	−16.4	**−13.8**
ICE	Heimay, Iceland	−23.7	10.4	**7.6**
IZO	Izana, Spain	−23.7	−13.8	**−10.0**
JFJ	Jungfraujoch, Switzerland	−24.9	**−0.4**	−23
KUM	Cape Kumukahi	−24.1	**−7.3**	−8.2
KZM	Plateau Assy, Kazakhstan	−22.5	**11.4**	17.8
MHD	Mace Head, Ireland	−25.0	**3.3**	4.3
MID	Sand Island, USA	−24.8	**−12.4**	−12.9
MLO	Mauna Loa, USA	−32.6	−16.8	**−14.6**
MNM	Minamitorishima, Japan	−15.1	**−2.4**	−6.1
NWR	Niwot Ridge, USA	−30.4	−11.6	**−9.2**
PAY	Payerne, Switzerland	−54.7	**−10.4**	−19.5
RIG	Rigi, Switzerland	**−14.2**	23.3	19.0
RPB	Ragged Point, Barbados	−15.9	−8.7	**-5.5**
RYO	Ryori, Japan	−44.1	**11.7**	20.5
SEY	Mahe Island, Seychelles	−5.2	−6.3	**3.2**
SHM	Shemya Island, USA	−32.7	**3.1**	3.8
SNB	Sonnblick, Austria	−77.2	**52.5**	−54.8
SMO	Cape Matatula, American Samoa	−6.6	−0.8	**−0.2**
UUM	Ulaan Uul, Mongolia	−29.1	**25.2**	27.2
WIS	Sede Boker, Israel	−22.9	**4.2**	22.5
WLG	Mt. Waliguan, China	−37.3	**−15.9**	19.8
ZEP	Ny-Alesund, Spitsbergen	−22.9	25.2	**22.5**
ALL		25.6	**11.6**	12.8

ACPD
12, 6909–6955, 2012

Table 4. Same as Table 3, but for the 6 stations chosen in the high-latitudes of the Southern Hemisphere.

Code	Location	Biais (ppb) Prior	MOPITT posterior	MOPITT-OMI posterior
CGO	Cape Grim, Australia	**12.5**	42.2	37.8
HBA	Halley Station, UK	**0.3**	11.1	9.1
PSA	Palmer Station, USA	**−0.4**	12.9	13.2
SPO	South Pole, USA	**1.1**	13.8	13.8
SYO	Syowa Station, Japan	**2.9**	17.2	18.0
TDF	Tierra del Fuego, Argentina	**−1.0**	13.1	13.5

ACPD
12, 6909–6955, 2012

Table 5. Total CH_4 emissions for years 2005 to 2008, before inversion and **after inversion**,and posterior mean over the 2005–2008 period for 14 continental regions and for the globe in $Tg\,CH_4\,yr^{-1}$. All budgets correspond to a 12-month period. The regional contributions to the global posterior mean are given in % (last column).

	2005		2006		2007		2008		Posterior mean	Contribution (%)
	Prior	Post	Prior	Post	Prior	Post	Prior	Post		
North Am Boreal	17	**18**	17	**19**	17	**20**	17	**19**	**19**	**4**
USA	50	**52**	50	**53**	50	**53**	50	**55**	**53**	**10**
South Am Trop	19	**20**	19	**19**	19	**20**	19	**20**	**20**	**4**
South Am Temp	53	**58**	50	**51**	54	**65**	50	**54**	**57**	**11**
Northern Africa	36	**43**	36	**41**	37	**48**	36	**49**	**45**	**9**
Southern Africa	18	**20**	17	**18**	18	**21**	18	**20**	**19**	**4**
Western Europe	35	**31**	35	**30**	35	**30**	35	**30**	**30**	**6**
Eastern Europe	31	**30**	31	**30**	31	**30**	31	**29**	**30**	**6**
Eurasian Boreal	28	**28**	29	**30**	28	**31**	29	**30**	**30**	**6**
Middle East	11	**11**	11	**11**	11	**11**	11	**12**	**11**	**2**
South Asia	63	**71**	63	**72**	63	**76**	63	**73**	**73**	**14**
South East Asia	84	**89**	84	**92**	86	**93**	84	**101**	**94**	**18**
Indonesia	35	**36**	34	**38**	32	**40**	32	**41**	**39**	**7**
Australia	11	**9**	11	**9**	11	**7**	11	**7**	**8**	**2**
Globe	491	**519**	490	**512**	491	**543**	486	**538**	**528**	**100**

ACPD
12, 6909–6955, 2012

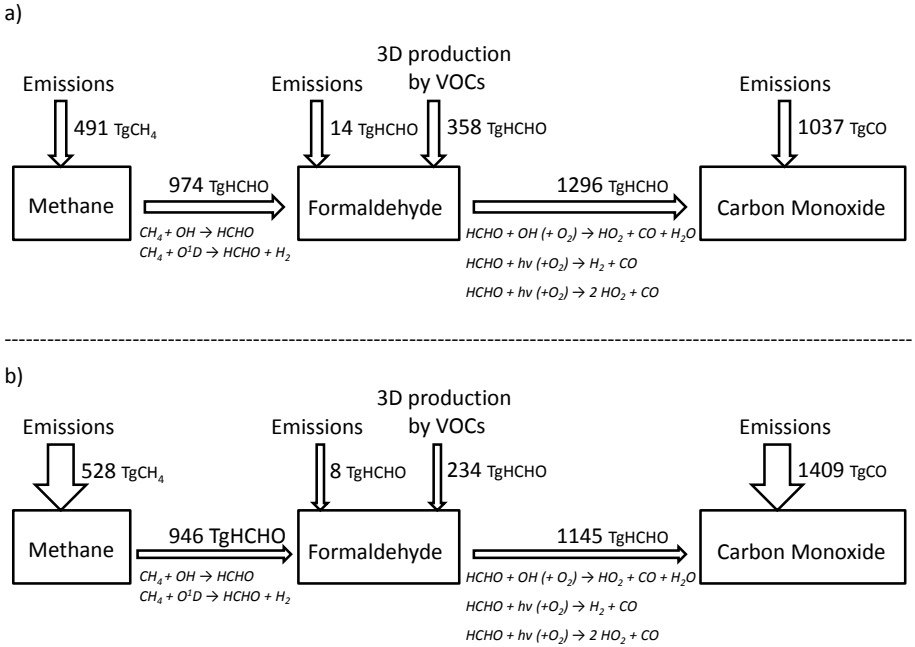

Fig. 1. Prior **(a)** and posterior **(b)** HCHO sources and sinks in the SACS mechanism. Sinks of CO and H_2, and the HCHO deposition are included in SACS but not displayed. Changes of arrow thickness between prior and posterior indicate a reduction or an increase of the sources and sinks. Values are averaged over the 2005–2008 time period.

ACPD
12, 6909–6955, 2012

Species	Types	Total number of observations	Number of observations per pixel and per month (July 2006)
			5 11 16 22 27 33 38 44 49 55
MCF	Surface stations	10,487	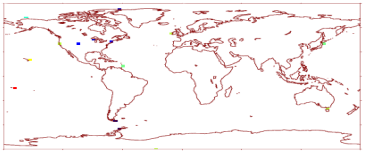
CH_4	Surface stations	201,174	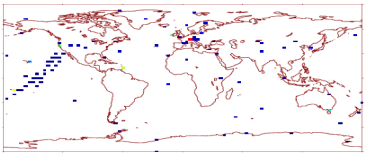
HCHO	OMI	4,443,425	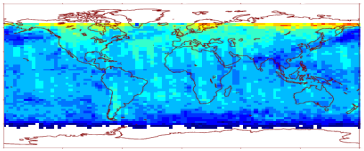
CO	MOPITT	4,759,828	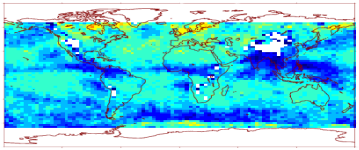

Fig. 2. Summary of the observations used in the inversion: total number of observations over the 2005–2008 time period and typical distributions of these observations on the right for July 2006.

ACPD
12, 6909–6955, 2012

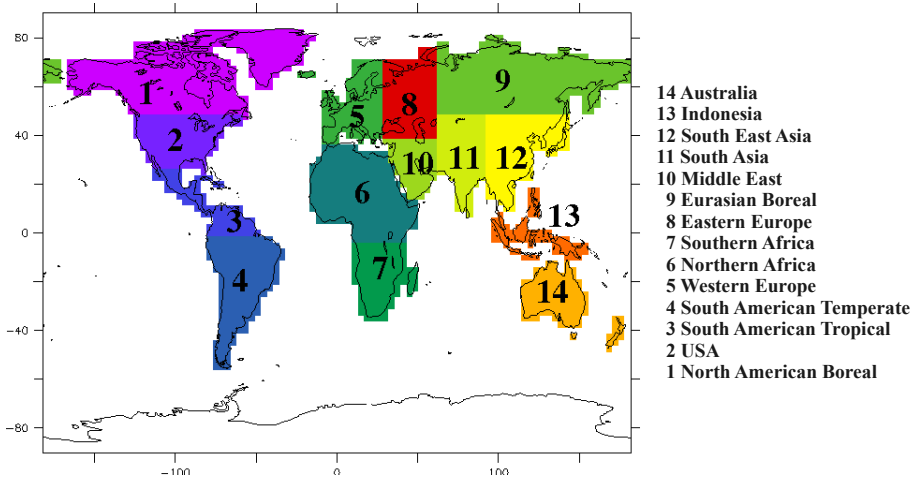

Fig. 3. Definition of the14 regions used in this study.

ACPD
12, 6909–6955, 2012

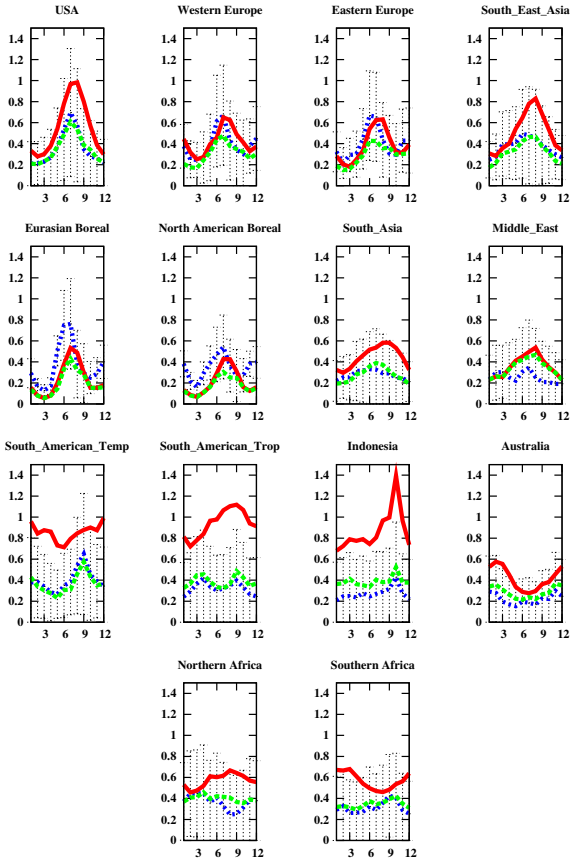

Fig. 4. Times series of monthly averaged formaldehyde total columns retrieved by OMI (in blue) and simulated by the model LMDz-SACS using the prior (in red) and the posterior fluxes (in green) for year 2006, from January to December. Error bars represent the OMI retrieval errors. Units are $10e^{16}$ molec cm^{-2}.

ACPD
12, 6909–6955, 2012

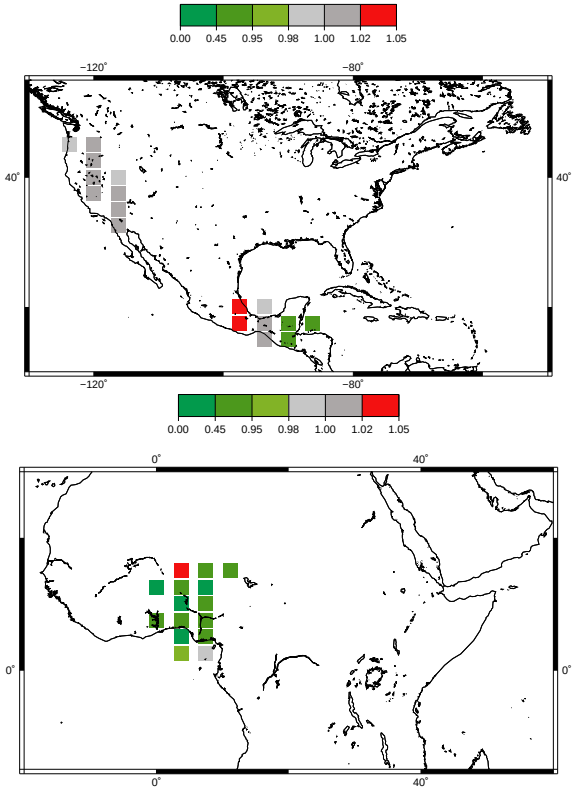

Fig. 5. Ratio of the posterior to the prior values of bias (in absolute value) between simulated and observed concentrations for the INTEX-B (top) and AMMA campaigns (bottom). The inversion improves the simulation when the ratio of the absolute bias is less than 1 (in green).

ACPD
12, 6909–6955, 2012

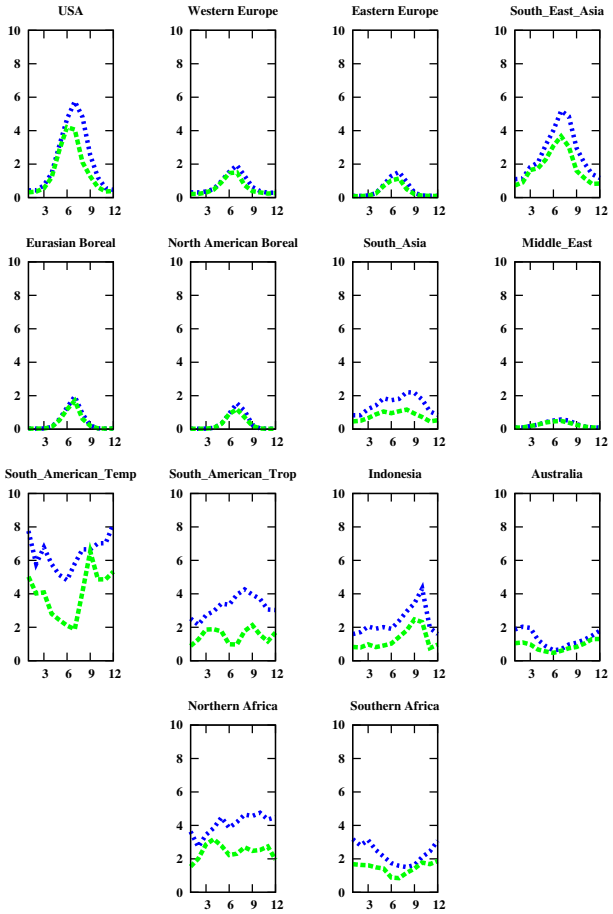

Fig. 6. Times series of prior (in blue) and posterior (in red) HCHO 3-D production by VOCs for year 2006. Units are Tg HCHO month^{-1}.

ACPD
12, 6909–6955, 2012

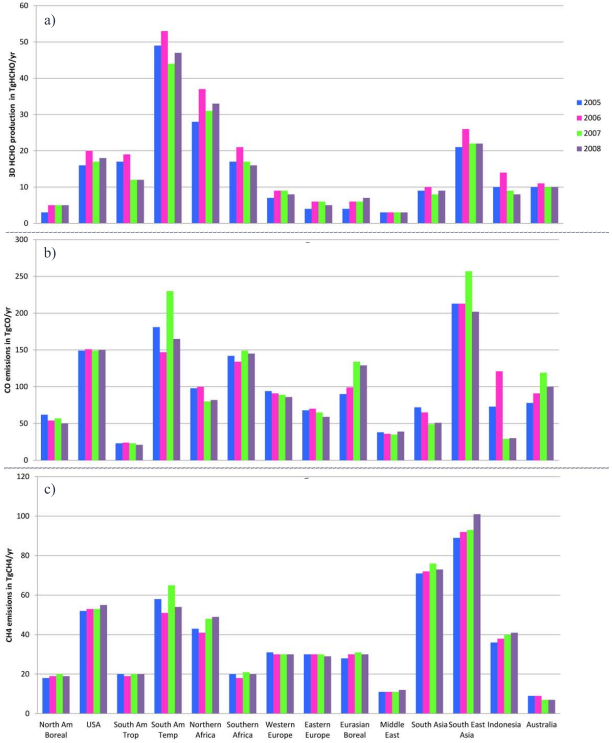

Fig. 7. Regional variations of the annual **(a)** posterior 3-D HCHO production by NMVOCs, **(b)** posterior CO emissions and **(c)** posterior CH_4 emissions, between 2005 and 2008.

ACPD
12, 6909–6955, 2012

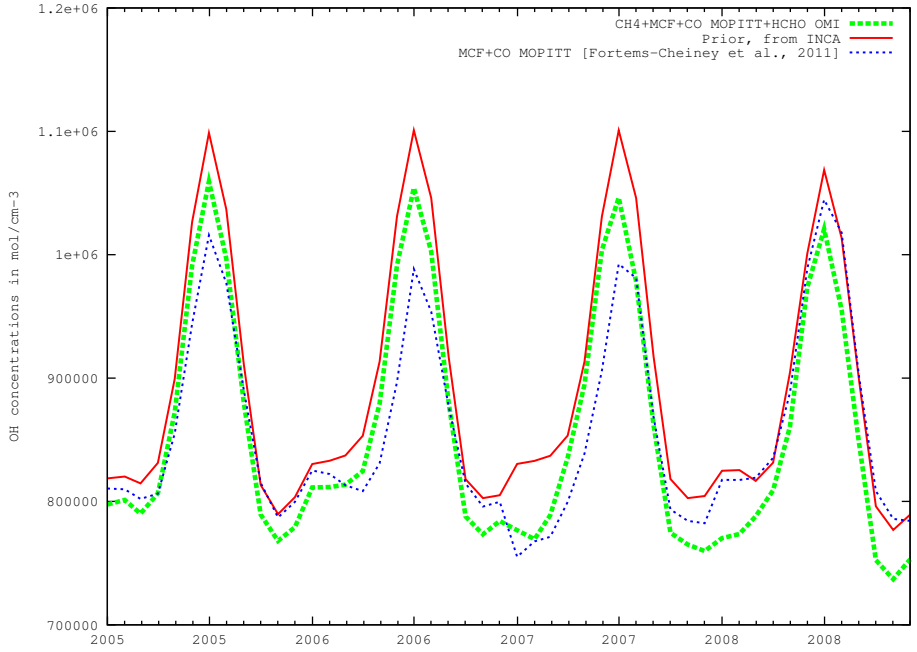

Fig. 8. Seasonal cycle of the global tropospheric mean of OH prior concentrations from LMDz-INCA (in red), OH posterior concentrations using only MOPITT as constraints from Fortems-Cheiney et al. (2011) (in blue) and OH posterior concentrations using OMI, MOPITT and surface stations (this study, in green), from January 2005 to December 2008. Units are mol cm^{-3}.

ACPD
12, 6909–6955, 2012

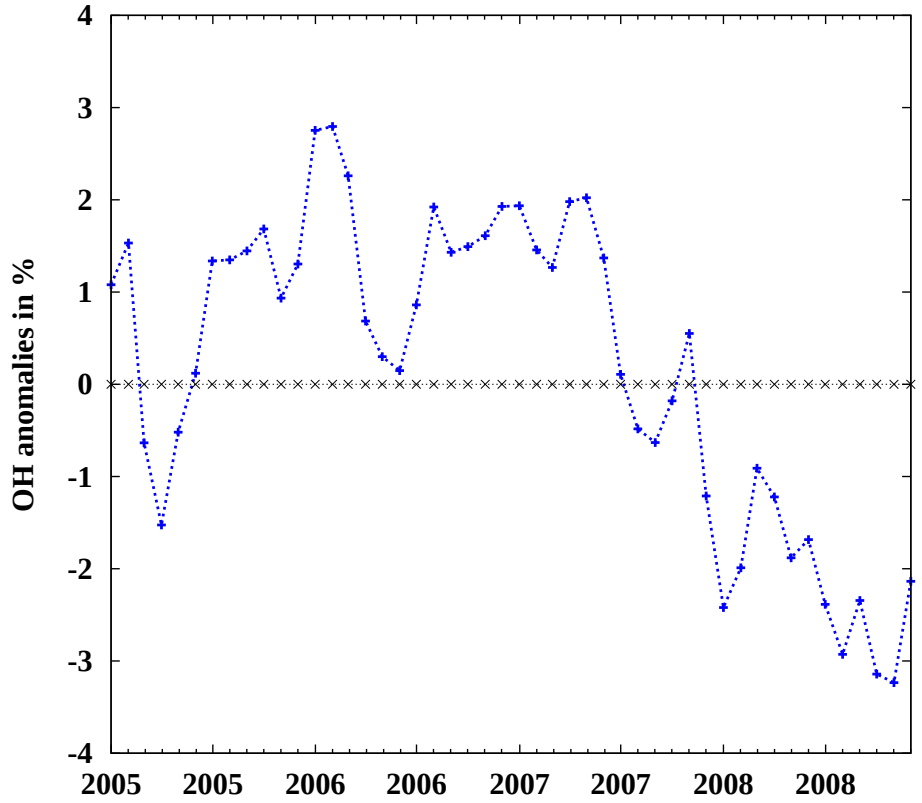

Fig. 9. Anomalies in global OH concentrations derived in our inversion from January 2005 to December 2008. Units are %.

ACPD
12, 6909–6955, 2012

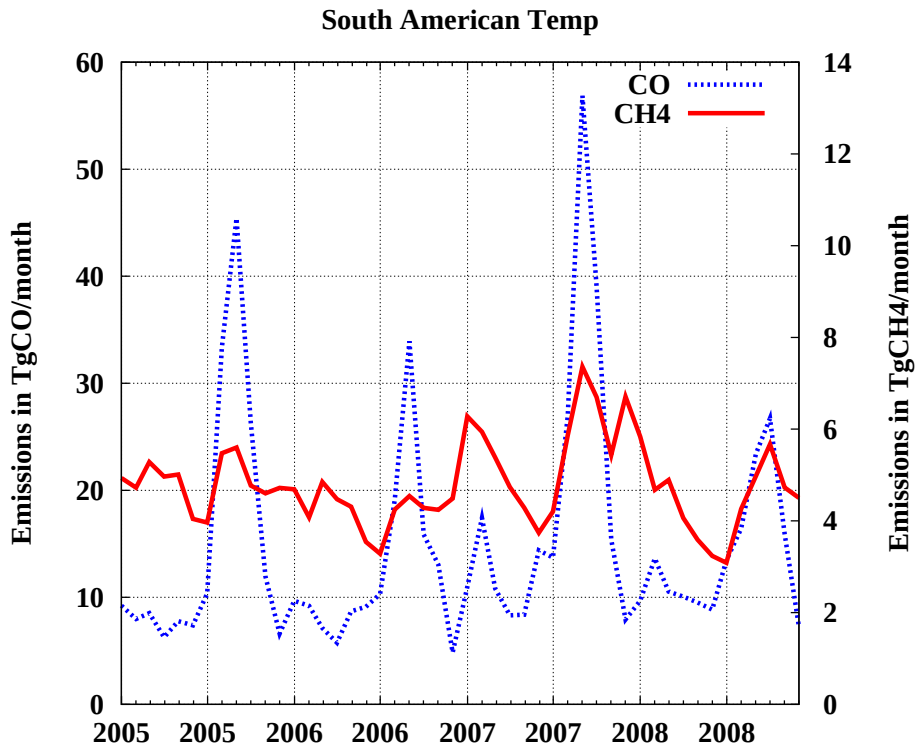

Fig. 10. Seasonal cycles of the posterior CO and CH_4 emissions for the tropical region South American Temperate, respectively in Tg CO month^{-1} and Tg CH_4 month^{-1}, from January 2005 to December 2008.

ACPD
12, 6909–6955, 2012